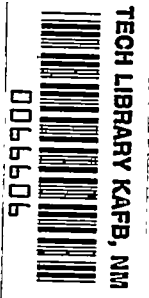


NACA TN 3515 5676

NACH
TN
3515
c.1



NATIONAL ADVISORY COMMITTEE FOR AERONAUTICS

TECHNICAL NOTE 3515

LOAN COPY: RETURN TO
AFWL TECHNICAL LIBRARY
KIRTLAND AFB, N. M.

ANALYSIS OF TWO-DIMENSIONAL COMPRESSIBLE-FLOW LOSS
CHARACTERISTICS DOWNSTREAM OF TURBOMACHINE

BLADE ROWS IN TERMS OF BASIC BOUNDARY-
LAYER CHARACTERISTICS

By Warner L. Stewart

Lewis Flight Propulsion Laboratory
Cleveland, Ohio



Washington

July 1955



TECHNICAL NOTE 3515

ANALYSIS OF TWO-DIMENSIONAL COMPRESSIBLE-FLOW LOSS CHARACTERISTICS

DOWNSTREAM OF TURBOMACHINE BLADE ROWS IN TERMS OF

BASIC BOUNDARY-LAYER CHARACTERISTICS

By Warner L. Stewart

SUMMARY

The effect of compressibility on the loss characteristics downstream of two-dimensional turbomachine blade rows is analyzed. Equations are derived for obtaining the compressible-flow boundary-layer characteristics for a simple power velocity distribution. Loss coefficients at the blade trailing edge are then obtained in terms of these characteristics. Finally, over-all loss coefficients, including the effect of mixing downstream of the blade row, are obtained in terms of these characteristics.

The blade loss coefficients based on kinetic energy both before and after mixing are approximately independent of compressibility effect, but the loss coefficients based on pressure are considerably affected. Thus, loss coefficients based on kinetic energy are the more desirable in describing the compressible-flow blade loss characteristics. The over-all loss coefficients also depend directly on the momentum thickness just at the blade trailing edge, indicating that an accurate determination of the blade loss characteristics depends on an accurate evaluation of the momentum thickness for compressible-flow conditions, either by experiment or theory.

The results of the analysis also indicate that the loss coefficients after mixing are significantly greater than the loss coefficients at the trailing edge, especially at high subsonic and supersonic velocity levels when based on pressure. This effect of mixing should therefore be included in describing the blade performance characteristics. The example discussed herein also indicates that increasing the trailing-edge thickness can increase the over-all loss coefficients significantly, with a compressibility effect only at flow angles close to axial.

3667

CK-1

INTRODUCTION

The potentialities of size, weight, and stage reduction in the rotating components of jet engines through utilization of increased flow velocities have motivated considerable research on these components. The practicability of such components in engines depends to a great extent on their ability to achieve efficiencies comparable to those of more conservative units. Thus, it is important that the effect of the increased flow velocities on the various losses within the turbomachine blade rows be understood.

One of the more important losses occurring within turbomachine blade rows is the two-dimensional friction loss incurred as the air passes over the blades. This loss is commonly described in terms of a mass-averaged total-pressure or kinetic-energy defect just at the blade exit. The measurements at the blade exit can also be used to obtain certain characteristics of the boundary layer as it leaves the blade. The characteristics commonly used in boundary-layer work are (1) displacement thickness, which is a measure of the flow blockage due to the boundary layer, (2) momentum thickness, which is a measure of the loss in momentum due to friction within the blade, and (3) energy thickness, which is a measure of the kinetic-energy loss due to friction.

After the flow leaves the blade, mixing takes place until uniform conditions are established. The over-all loss as obtained from the blade inlet to that station after mixing represents the true loss of the blade and is greater than that obtained by mass-averaging the loss just at the blade exit. The difference between the two losses can be termed a mixing loss, since it occurs as a result of the nonuniformities of the flow just at the blade trailing edge.

This report presents an analysis of the losses occurring downstream of a two-dimensional blade row in terms of the basic boundary-layer characteristics occurring at the blade exit for compressible-flow conditions. Equations are derived for the following:

- (1) Obtaining the compressible-flow characteristics of a boundary layer having a simple power velocity profile
- (2) Using these boundary-layer characteristics in obtaining loss coefficients at the blade trailing edge
- (3) Again using these boundary-layer characteristics in obtaining over-all loss coefficients, which include the effect of mixing downstream of the blade row.

The results of the analysis are then used (1) to show the effect of increasing the flow velocities into the high subsonic and supersonic region on the loss coefficients, (2) to study the effect of mixing

downstream of the blade row on the loss coefficients, and (3) to study the effect of trailing-edge thickness on the over-all loss coefficients.

BASIC CONSIDERATIONS

A description of the basic considerations involved in this investigation can be made through use of figure 1. A typical two-dimensional turbomachine blade row with the station nomenclature used in the analysis is shown in figure 1(a). All symbols are defined in appendix A.

Station 0

Station 0 represents the inlet to the blade row. At this station uniform total pressure p_0^t is assumed to occur. No flow angle or velocity level need be specified at this station, as the investigation presented herein is independent of these quantities.

Station 1

Station 1 is that station just downstream of the blade row. As the flow passes through the blade row, a boundary layer is formed on each surface. This boundary layer results in a velocity and total-pressure profile similar to those indicated in figure 1(c). The velocity varies from that at free stream ($V_{fs,1}$) to 0 in the region of the trailing edge. The total pressure varies from a free-stream value of $p_{fs,1}^t = p_0^t$ to the static pressure p_1 . As indicated by figure 1(c), this static pressure is assumed constant across station 1.

Also shown at this station is a trailing-edge blockage δ_{te} , which is expressed in terms of spacing s . As indicated by figure 1(b), the value of δ_{te} can be obtained from the relation

$$\delta_{te} = \frac{t}{s \cos \alpha_1} \quad (1)$$

It is assumed that over this area no weight flow, and hence no velocity, occurs and also that the static pressure is equal to p_1 .

3667

CK-1 back

Station 2

Station 2 is located at a distance sufficiently downstream of the blade row that complete mixing has taken place. Both flow velocity V_2 and total pressure p_2' are uniform, as shown in figure 1(c). The total pressure p_2' is less than p_0' because of the blade loss.

The investigation presented herein utilizes the basic considerations just discussed in the following three phases:

(1) The compressible-flow boundary-layer characteristics occurring at station 1 are developed for a simple power velocity profile.

(2) Loss coefficients at station 1 are then obtained in terms of these boundary-layer characteristics.

(3) Over-all loss coefficients at station 2 are then obtained in terms of these same boundary-layer characteristics at station 1.

The three phases are presented in this order in the next three sections.

BASIC BOUNDARY-LAYER CHARACTERISTICS

Four parameters are used in this report to describe the characteristics of the boundary layer at the blade exit: (1) displacement thickness, (2) momentum thickness, (3) energy thickness, and (4) pressure thickness. The first three parameters have been used previously in one form or another in boundary-layer work. The fourth parameter is the same as the third for incompressible flow and is a measure of the mass-averaged total-pressure loss at the exit of the blade row for compressible flow.

Displacement Thickness

A typical boundary-layer velocity profile is shown in figure 2. The velocity varies from zero on the surface to V_{fs} at the full boundary-layer height δ_{full} . The free-stream static pressure is assumed to extend through this boundary layer to the wall, and the total temperature is assumed constant across the boundary layer. The loss in mass flow as a

result of the boundary-layer formation is expressed in terms of a displacement thickness δ , over which free-stream specific mass flow passes. Mathematically,

$$\delta \rho_{fs} V_{fs} = \delta_{full} \rho_{fs} V_{fs} - \int_0^{\delta_{full}} \rho V \, dY$$

or

$$\delta = \delta_{full} - \int_0^{\delta_{full}} \frac{\rho V}{\rho_{fs} V_{fs}} \, dY \quad (2)$$

Momentum Thickness

The momentum thickness θ is defined in a manner similar to the displacement thickness. The loss in momentum as a result of surface friction is expressed in terms of a length θ over which free-stream momentum passes; that is,

$$\theta \rho_{fs} V_{fs}^2 = V_{fs} \int_0^{\delta_{full}} \rho V \, dY - \int_0^{\delta_{full}} \rho V^2 \, dY$$

or

$$\theta = \int_0^{\delta_{full}} \frac{\rho V}{\rho_{fs} V_{fs}} \, dY - \int_0^{\delta_{full}} \frac{\rho V^2}{\rho_{fs} V_{fs}^2} \, dY \quad (3)$$

Energy Thickness

The loss in kinetic energy as a result of surface friction is similarly expressed in terms of a length ψ over which free-stream kinetic energy passes; that is,

$$\psi \frac{1}{2} \rho_{fs} V_{fs}^3 = \frac{1}{2} V_{fs}^2 \int_0^{\delta_{full}} \rho V \, dY - \frac{1}{2} \int_0^{\delta_{full}} \rho V^3 \, dY$$

or

$$\psi = \int_0^{\delta_{full}} \frac{\rho V}{\rho_{fs} V_{fs}} dY - \int_0^{\delta_{full}} \frac{\rho V^3}{\rho_{fs} V_{fs}^3} dY \quad (4)$$

Pressure Thickness

Finally, the mass-integrated loss in total pressure as a result of surface friction is expressed in terms of a length ξ over which a mass-integrated free-stream dynamic pressure exists. Mathematically,

$$\xi \rho_{fs} V_{fs} (p_{fs}' - p) = p_{fs}' \int_0^{\delta_{full}} \rho V dY - \int_0^{\delta_{full}} p' \rho V dY$$

or,

$$\xi = \frac{\int_0^{\delta_{full}} \frac{\rho V}{\rho_{fs} V_{fs}} dY - \int_0^{\delta_{full}} \frac{p'}{p_{fs}'} \frac{\rho V}{\rho_{fs} V_{fs}} dY}{1 - \frac{p}{p_{fs}'}} \quad (5)$$

Form Factor

The form factor H is defined as

$$H = \frac{\delta}{\theta} \quad (6)$$

Substituting equations (2) and (3) into equation (6) gives

$$H = \frac{\delta_{full} - \int_0^{\delta_{full}} \frac{\rho V}{\rho_{fs} V_{fs}} dY}{\int_0^{\delta_{full}} \frac{\rho V}{\rho_{fs} V_{fs}} dY - \int_0^{\delta_{full}} \frac{\rho V^2}{\rho_{fs} V_{fs}^2} dY}$$

or, defining $y = Y/\delta_{full}$,

$$H = \frac{1 - \int_0^1 \frac{\rho V}{\rho_{fs} V_{fs}} dy}{\int_0^1 \frac{\rho V}{\rho_{fs} V_{fs}} dy - \int_0^1 \frac{\rho V^2}{\rho_{fs} V_{fs}^2} dy} \quad (7)$$

Energy Factor

The energy factor E is defined as

$$E = \frac{\Psi}{\theta} \quad (8)$$

Substituting equations (3) and (4) into equation (8) with $y = Y/\delta_{full}$,

$$E = \frac{\int_0^1 \frac{\rho V}{\rho_{fs} V_{fs}} dy - \int_0^1 \frac{\rho V^3}{\rho_{fs} V_{fs}^3} dy}{\int_0^1 \frac{\rho V}{\rho_{fs} V_{fs}} dy - \int_0^1 \frac{\rho V^2}{\rho_{fs} V_{fs}^2} dy} \quad (9)$$

Pressure Factor

A pressure factor P is defined herein as

$$P = \frac{\xi}{\theta} \quad (10)$$

Substituting equations (3) and (5) into equation (10) with $y = Y/\delta_{full}$,

$$P = \frac{\int_0^1 \frac{\rho V}{\rho_{fs} V_{fs}} dy - \int_0^1 \frac{p'}{p'_{fs}} \frac{\rho V}{\rho_{fs} V_{fs}} dy}{\left[1 - \left(\frac{p}{p'}\right)_{fs}\right] \left(\int_0^1 \frac{\rho V}{\rho_{fs} V_{fs}} dy - \int_0^1 \frac{\rho V^2}{\rho_{fs} V_{fs}^2} dy \right)} \quad (11)$$

Effect of Compressibility on H, E, and P

A velocity profile commonly used in boundary-layer work is what is called the simple power profile. This relation is

$$\frac{V}{V_{fs}} = y^n \quad (12)$$

This velocity profile is applied to equations (7), (9), and (11) in appendix B to determine the effect of compressibility on H, E, and P. The resulting equations derived in appendix B are

$$H = \frac{\frac{1}{n+1} + \frac{3A_{fs}}{3n+1} + \frac{5A_{fs}^2}{5n+1} + \dots}{\frac{1}{(n+1)(2n+1)} + \frac{A_{fs}}{(3n+1)(4n+1)} + \frac{A_{fs}^2}{(5n+1)(6n+1)} + \dots} \quad (B12)$$

$$E = \frac{2 \left[\frac{1}{(n+1)(3n+1)} + \frac{A_{fs}}{(3n+1)(5n+1)} + \frac{A_{fs}^2}{(5n+1)(7n+1)} + \dots \right]}{\frac{1}{(n+1)(2n+1)} + \frac{A_{fs}}{(3n+1)(4n+1)} + \frac{A_{fs}^2}{(5n+1)(6n+1)} + \dots} \quad (B13)$$

$$P = \frac{\frac{1 - \left(\frac{p}{p^*}\right)_{fs}}{n+1} + \frac{A_{fs} \left[1 - \left(\frac{p}{p^*}\right)_{fs} B\right]}{3n+1} + \frac{A_{fs}^2 \left[1 - \left(\frac{p}{p^*}\right)_{fs} \frac{B(B+1)}{2!}\right]}{5n+1} + \dots}{n \left[1 - \left(\frac{p}{p^*}\right)_{fs}\right] \left[\frac{1}{(n+1)(2n+1)} + \frac{A_{fs}}{(3n+1)(4n+1)} + \frac{A_{fs}^2}{(5n+1)(6n+1)} + \dots \right]} \quad (B14)$$

where $A_{fs} = \frac{\gamma-1}{\gamma+1} \left(\frac{V}{V_{cr}}\right)_{fs}^2$ and $B = \frac{2\gamma-1}{\gamma-1}$. As $\left(\frac{V}{V_{cr}}\right)_{fs} \rightarrow 0$, the expressions

$$H \left(\frac{V}{V_{cr}}\right)_{fs} \rightarrow 0 = 2n+1 \quad (B15)$$

and

$$E \left(\frac{V}{V_{cr}}\right)_{fs} \rightarrow 0 = P \left(\frac{V}{V_{cr}}\right)_{fs} \rightarrow 0 = \frac{2(2n+1)}{3n+1} \quad (B16)$$

are obtained. These expressions are identical with those obtained considering air incompressible. Also, as $n \rightarrow 0$, the expressions

$$H_{n \rightarrow 0} = \frac{1 + A_{fs}}{1 - A_{fs}} \quad (B17)$$

$$E_{n \rightarrow 0} = 2 \quad (B18)$$

and

$$P_{n \rightarrow 0} = 2 \left[\frac{\frac{\gamma}{\gamma-1} A_{fs}}{(1 - A_{fs}) - (1 - A_{fs})^{\frac{2\gamma-1}{\gamma-1}}} \right] \quad (B19)$$

are obtained.

The parameters H , E , and P , which were computed from equations (B12) to (B19) for a range of free-stream critical velocity ratio $(V/V_{cr})_{fs}$ and velocity power n , are shown in figure 3. The energy

3667
CK-2

factor E is plotted as a function of form factor H with $(V/V_{cr})_{fs}$ and n as parameters in figure 3(a). For a given n , the form factor increases as the flow velocity is increased into the high subsonic and supersonic range. For example, at $n \rightarrow 0$ the limiting H increases from 1 at $(V/V_{cr})_{fs} \rightarrow 0$ to approximately 2 at $(V/V_{cr})_{fs} = 1.4$. The energy factor E is almost independent of velocity level for a specified n . At $n \rightarrow 0$, E is constant and equal to 2. At $n = 0.5$, E increases from 1.60 at $(V/V_{cr})_{fs} \rightarrow 0$ to only 1.62 at $(V/V_{cr})_{fs} = 1.4$, an increase of only 1 percent. The importance of this near independence of velocity level is brought out later in the report.

The pressure factor P is plotted as a function of H in figure 3(b). The curve representing $(V/V_{cr})_{fs} \rightarrow 0$ is the same in both figures, since $E \left(\frac{V}{V_{cr}} \right)_{fs} \rightarrow 0 = P \left(\frac{V}{V_{cr}} \right)_{fs} \rightarrow 0$. However, as the flow velocity is

raised into the high subsonic and supersonic region, the pressure factor P increases markedly. For example, at $n \rightarrow 0$, P increases from 2 at $(V/V_{cr})_{fs} \rightarrow 0$ to 2.97 at $(V/V_{cr})_{fs} = 1$ and 4.54 at $(V/V_{cr})_{fs} = 1.4$. The importance of this dependence of P on velocity level is also discussed in later sections.

APPLICATION OF BASIC BOUNDARY-LAYER CHARACTERISTICS TO

LOSS COEFFICIENTS AT BLADE EXIT (STATION 1)

The basic boundary-layer characteristics described in the previous section are now used in obtaining the kinetic-energy-loss coefficient \bar{e}_1 and pressure-loss coefficient $\bar{\omega}_1$. The kinetic-energy-loss coefficient

$$\bar{e}_1 = 1 - \frac{(\overline{V^2})_1}{V_{th,1}^2} = 1 - \frac{(\overline{V^2})_1}{V_{fs,1}^2} \quad (13)$$

and represents the mass-averaged loss in kinetic energy at station 1. Similarly,

$$\bar{\omega}_1 = \frac{1 - \frac{\overline{P_1}}{P_0}}{1 - \frac{\overline{P_1}}{P_0}} = \frac{1 - \frac{\overline{P_1}}{P_{fs,1}}}{1 - \frac{\overline{P_1}}{P_{fs,1}}} \quad (14)$$

and represents the mass-averaged loss in total pressure at station 1.

Expanding equations (13) and (14),

$$\bar{e}_1 = \frac{\int_0^1 \left[1 - \left(\frac{V}{V_{fs}} \right)_1^2 \right] \left(\frac{\rho V}{\rho_{fs} V_{fs}} \right)_1 d\left(\frac{u}{s}\right)}{\int_0^1 \left(\frac{\rho V}{\rho_{fs} V_{fs}} \right)_1 d\left(\frac{u}{s}\right)} \quad (15)$$

and

$$\bar{\omega}_1 = \frac{\int_0^1 \left[1 - \left(\frac{p'}{p_{fs}} \right)_1 \right] \left(\frac{\rho V}{\rho_{fs} V_{fs}} \right)_1 d\left(\frac{u}{s}\right)}{\left[1 - \left(\frac{p}{p_{fs}} \right)_1 \right] \int_0^1 \left(\frac{\rho V}{\rho_{fs} V_{fs}} \right)_1 d\left(\frac{u}{s}\right)} \quad (16)$$

In order to express these quantities in terms of the basic boundary-layer characteristics, define

$$\int_0^1 \left(\frac{\rho V}{\rho_{fs} V_{fs}} \right)_1 d\left(\frac{u}{s}\right) \equiv 1 - \delta^* - \delta_{te} \quad (17a)$$

$$\int_0^1 \left[1 - \left(\frac{V}{V_{fs}} \right)_1 \right] \left(\frac{\rho V}{\rho_{fs} V_{fs}} \right)_1 d\left(\frac{u}{s}\right) \equiv \theta^* \quad (17b)$$

$$\int_0^1 \left[1 - \left(\frac{V}{V_{fs}} \right)_1^2 \right] \left(\frac{\rho V}{\rho_{fs} V_{fs}} \right)_1 d\left(\frac{u}{s}\right) \equiv \psi^* \quad (17c)$$

3667

CK-2 back

$$\int_0^1 \frac{\left[1 - \left(\frac{p'}{p_{fs}}\right)_1\right] \left(\frac{\rho V}{\rho_{fs} V_{fs}}\right)_1 d\left(\frac{u}{s}\right)}{1 - \left(\frac{p}{p_{fs}}\right)_1} \equiv \xi^* \quad (17d)$$

where it is assumed that

$$\delta^* = \frac{\delta_{tot}}{s \cos \alpha_1} = \frac{\delta_s + \delta_p}{s \cos \alpha_1} \quad (18a)$$

$$\theta^* = \frac{\theta_{tot}}{s \cos \alpha_1} = \frac{\theta_s + \theta_p}{s \cos \alpha_1} \quad (18b)$$

$$\psi^* = \frac{\psi_{tot}}{s \cos \alpha_1} = \frac{\psi_s + \psi_p}{s \cos \alpha_1} \quad (18c)$$

$$\xi^* = \frac{\xi_{tot}}{s \cos \alpha_1} = \frac{\xi_s + \xi_p}{s \cos \alpha_1} \quad (18d)$$

Substituting equations (17) into equations (15) and (16) then yields

$$\bar{e}_1 = \frac{\psi^*}{1 - (\delta^* + \delta_{te})} \quad (19)$$

and

$$\bar{\omega}_1 = \frac{\xi^*}{1 - (\delta^* + \delta_{te})} \quad (20)$$

Defining

$$\left. \begin{aligned} E^* &\equiv \frac{\psi_{tot}}{\theta_{tot}} = \frac{\psi^*}{\theta^*} \\ P^* &\equiv \frac{\xi_{tot}}{\theta_{tot}} = \frac{\xi^*}{\theta^*} \end{aligned} \right\} \quad (21)$$

and

equations (19) and (20) can be written as

$$\bar{e}_1 = \frac{\theta^* E^*}{1 - (\delta^* + \delta_{te})} \quad (22)$$

$$\bar{\omega}_1 = \frac{\theta^* P^*}{1 - (\delta^* + \delta_{te})} \quad (23)$$

APPLICATION OF BASIC BOUNDARY-LAYER CHARACTERISTICS TO OVER-ALL

LOSS COEFFICIENTS (STATION 2)

This section presents the equations used to obtain the over-all loss coefficients across the blade row \bar{e}_2 and $\bar{\omega}_2$. Although the bars again denote a mass-averaged value, actual mass-averaging is not necessary, since conditions are uniform at station 2. These coefficients are defined in the same manner as \bar{e}_1 and $\bar{\omega}_1$; that is,

$$\bar{e}_2 = 1 - \frac{V_2^2}{V_{th,2}^2} = \frac{\left(\frac{P_0'}{P_2'}\right)^{\frac{\gamma-1}{\gamma}} - 1}{\left(\frac{P_0'}{P_2'}\right)^{\frac{\gamma-1}{\gamma}} - 1} \quad (24)$$

and

$$\bar{\omega}_2 = \frac{1 - \frac{P_2'}{P_0'}}{1 - \frac{P_2}{P_0}} \quad (25)$$

The derivation of the equations used in obtaining these coefficients in terms of the basic boundary-layer characteristics at station 1 is presented in appendix C.

Incompressible Flow

For the incompressible-flow case, which represents the lower limit of the compressible-flow case where $(V/V_{cr})_{fs,1} \rightarrow 0$, the density ρ is

constant. Because of this specification, $\bar{e}_2, \left(\frac{V}{V_{cr}}\right)_{fs} \rightarrow 0 = \bar{\omega}_2, \left(\frac{V}{V_{cr}}\right)_{fs} \rightarrow 0$ and can be set up directly in terms of the boundary-layer characteristics at station 1. This is done in appendix C, and rewritten here is

$$\begin{aligned} \bar{e}_2, \left(\frac{V}{V_{cr}}\right)_{fs,1} \rightarrow 0 &= \bar{\omega}_2, \left(\frac{V}{V_{cr}}\right)_{fs,1} \rightarrow 0 \\ &= 1 - \frac{\sin^2 \alpha_1 \frac{(1 - \delta^* - \delta_{te} - \theta^*)^2}{(1 - \delta^* - \delta_{te})^2} + \cos^2 \alpha_1 (1 - \delta^* - \delta_{te})^2}{1 + 2 \cos^2 \alpha_1 [(1 - \delta^* - \delta_{te})^2 - (1 - \delta^* - \delta_{te} - \theta^*)^2]} \end{aligned} \quad (C11)$$

where

$$\delta_{te} + \delta^* = \frac{t + \delta_{tot}}{s \cos \alpha_1}$$

Compressible Flow

For the compressible-flow case, the density ρ varies and must be considered in the derivation. When this was done, no explicit equation for \bar{e}_2 or $\bar{\omega}_2$ could be obtained as for incompressible flow. However, from equations (24) and (25), it is evident that, once p_2'/p_0' and p_2/p_2' are known for a given set of conditions, \bar{e}_2 and $\bar{\omega}_2$ can be computed easily. The following steps summarize the method of computing these pressure ratios described in appendix C for given conditions at the blade exit:

- (1) The parameters C and D are computed from

$$C \equiv \frac{(1 - A_{fs,1}) \frac{\gamma + 1}{2\gamma} + \cos^2 \alpha_1 (1 - \delta^* - \delta_{te} - \theta^*) \left(\frac{V}{V_{cr}}\right)_{fs,1}^2}{\cos \alpha_1 (1 - \delta^* - \delta_{te}) \left(\frac{V}{V_{cr}}\right)_{fs,1}} \quad (C16)$$

$$D \equiv \left(\frac{V}{V_{cr}} \right)_{fs,1} \sin \alpha_1 \left(\frac{1 - \delta^* - \delta_{te} - \theta^*}{1 - \delta^* - \delta_{te}} \right) \quad (C18)$$

(2) The quantity $(V_x/V_{cr})_2$ is obtained from the equation

$$\left(\frac{V_x}{V_{cr}} \right)_2 = \frac{\gamma C}{\gamma + 1} - \sqrt{\left(\frac{\gamma C}{\gamma + 1} \right)^2 - 1 + \frac{\gamma - 1}{\gamma + 1} D^2} \quad (C20)$$

(3) The density ratio $(\rho/\rho')_2$ is computed from

$$\left(\frac{\rho}{\rho'} \right)_2 = \left\{ 1 - \frac{\gamma - 1}{\gamma + 1} \left[D^2 + \left(\frac{V_x}{V_{cr}} \right)_2^2 \right] \right\}^{\frac{1}{\gamma - 1}} \quad (C21)$$

(4) The total-pressure ratio p'_2/p'_0 is computed from

$$\frac{p'_2}{p'_0} = \frac{\left(\frac{\rho V}{\rho' V_{cr}} \right)_{fs,1} \cos \alpha_1 (1 - \delta^* - \delta_{te})}{\left(\frac{\rho V_x}{\rho' V_{cr}} \right)_2} \quad (C22)$$

(5) The pressure ratio $(p/p')_2$ can be computed from step (3) and the equation

$$\left(\frac{p}{p'} \right)_2 = \left(\frac{\rho}{\rho'} \right)_2^\gamma$$

(6) Once this pressure ratio is known, \bar{e}_2 and $\bar{\omega}_2$ can easily be computed from equations (24) and (25).

The equations just presented were used to obtain the curves in figure 4. Figure 4(a), obtained from equation (C11), represents the limiting case where $(V/V_{cr})_{fs,1} \rightarrow 0$. Figures 4(b) to (e) were obtained from the compressible-flow equations and cover $(V/V_{cr})_{fs,1}$ of 0.6, 1.0, 1.2, and 1.4, respectively.

Except for figures 4(d) and (e) (supersonic flow), each figure has three parts corresponding to α_1 of 0° , 30° , and 60° . For $(V/V_{cr})_{fs,1}$ of 1.2 and 1.4 (figs. 4(d) and (e)), a limitation is imposed

on α_1 (37.5° for 1.2 and 50° for 1.4). These angles represent the limit where the axial component of the Mach number $M_{fs,1}$ is unity. At angles less than these limits, an oblique or normal shock was indicated in the solution to the equations. Figure 5 presents this limiting angle α_1 as a function of the supersonic $(V/V_{cr})_{fs,1}$. Thus, there are only two parts for figures 4(d) and (e), corresponding to α_1 of 37.5° and 60° for $(V/V_{cr})_{fs,1} = 1.2$ and 50° and 60° for $(V/V_{cr})_{fs,1} = 1.4$.

Shown in each figure are the over-all kinetic-energy-loss coefficient \bar{e}_2 and the pressure-loss coefficient \bar{w}_2 as functions of the momentum thickness θ^* for a range of $(t + \delta_{tot})/s$ from a lower limit to 0.10. This lower limit as shown represents the minimum $(t + \delta_{tot})/s$ that can be obtained for the given α_1 and θ^* and is computed using the minimum form factor from the equation

$$\frac{t + \delta_{tot}}{s} = (\cos \alpha_1) \theta^* \quad H_{n \rightarrow 0}$$

where $H_{n \rightarrow 0}$ is obtained from equation (B17).

Also shown in the figures are lines representing

$$\theta^* \quad E_{n \rightarrow 0} = 2\theta^* \quad (26)$$

and

$$\theta^* \quad P_{n \rightarrow 0} \quad (27)$$

as a function of θ^* . The significance of these curves is discussed later.

For specified boundary-layer characteristics and blade geometry, figure 4 can be used in estimating the over-all loss coefficients \bar{e}_2 and \bar{w}_2 for any blade given conditions at station 1. The figure can also be used to study the kinetic-energy and pressure defects behind a blade row with satisfactory accuracy for moderate values of $(t + \delta_{tot})/s$. This can be done using p_1 and $V_{fs,1}$ instead of p_2 and $V_{th,2}$ in equations (24) and (25). Further, the figure can be used to make some general observations concerning the flow conditions downstream of the blade.

Accuracy of Boundary-Layer Characteristics Needed to Compute Over-All Loss Coefficients

In determining the over-all loss coefficients of a blade of a given geometry, the boundary-layer characteristics at the blade exit, θ^* and $(t + \delta_{tot})/s$, must be known or estimated. Inspection of figure 4 shows that, especially for small values of $(t + \delta_{tot})/s$, only moderate accuracy in obtaining this parameter need be required. However, since \bar{e}_2 and $\bar{\omega}_2$ are almost directly proportional to θ^* , the accuracy in obtaining these coefficients depends on the accuracy in knowing θ^* . Now,

$$\theta^* = \frac{\theta_{tot}}{s \cos \alpha_1} \quad (18b)$$

Since s and α_1 are functions of geometry, the accuracy in obtaining θ^* in turn directly depends on the accuracy in obtaining the total momentum thickness θ_{tot} . It is thus necessary to have either (1) extensive data available from which accurate estimates of the momentum thickness can be obtained or (2) an accurate analytical method for computing the momentum thickness in terms of the blade geometry and velocity and static-pressure distributions around the blade for compressible-flow conditions, before an accurate evaluation of the blade over-all loss characteristics can be made.

Effect of Compressibility on Loss Coefficients Before and After Mixing

A study of the effect of compressibility on the loss coefficients before and after mixing can be made from figure 4 and equations (22) and (23). If $\delta^* + \delta_{te}$ is sufficiently small, the equations can be modified to

$$\bar{e}_1 \approx \theta^* E^* \quad (28)$$

$$\bar{\omega}_1 \approx \theta^* P^* \quad (29)$$

Inspection of figure 4 shows that the lines representing $\theta^* \xrightarrow{n \rightarrow 0} E$ (eq. (26)) and the lines representing $\theta^* \xrightarrow{n \rightarrow 0} P$ (eq. (27)) approxi-

mate \bar{e}_2 and $\bar{\omega}_2$ for small values of $(t + \delta_{tot})/s$. So, from equations (26) to (29),

3667

3-20

$$\frac{\bar{e}_2}{\bar{e}_1} \approx \frac{E_n \rightarrow 0}{E^*} \quad (30)$$

$$\frac{\bar{\omega}_2}{\bar{\omega}_1} \approx \frac{P_n \rightarrow 0}{P^*} \quad (31)$$

In illustrating the effect of compressibility on these loss coefficients, let the factors E^* and P^* be represented by E and P corresponding to $n = 0.25$. With this assumption figure 3 can be used to compute the ratios \bar{e}_2/\bar{e}_1 and $\bar{\omega}_2/\bar{\omega}_1$ from equations (30) and (31). The calculation results are shown in figure 6, where \bar{e}_2/\bar{e}_1 and $\bar{\omega}_2/\bar{\omega}_1$ are shown as functions of free-stream critical velocity ratio at station 1, $(V/V_{cr})_{fs,1}$. At $(V/V_{cr})_{fs,1} \rightarrow 0$, the values of \bar{e}_2/\bar{e}_1 and $\bar{\omega}_2/\bar{\omega}_1$ are identical and in this case equal to 1.16. Thus, for $(V/V_{cr})_{fs,1} \rightarrow 0$, a 16-percent increase in loss coefficient is obtained because of the mixing downstream of the blade row.

As the flow velocities are increased into the high subsonic and supersonic range, \bar{e}_2/\bar{e}_1 remains practically constant, indicating that the effect of mixing on the kinetic-energy-loss coefficient is almost independent of velocity level. However, $\bar{\omega}_2/\bar{\omega}_1$ increases markedly as the velocity level is increased, from 1.16 at $(V/V_{cr})_{fs,1} \rightarrow 0$ to 1.39 at $(V/V_{cr})_{fs,1} = 1.0$ and 1.70 at $(V/V_{cr})_{fs,1} = 1.4$. These same trends can, of course, be observed in figure 4, in that the curves for $\bar{\omega}_2$ increase markedly in slope from those of \bar{e}_2 as the velocity level is increased. On the basis of this discussion, it can be concluded that, using either \bar{e}_2 or $\bar{\omega}_2$, mixing downstream of the blade results in loss coefficients significantly greater than those at the trailing edge, $\bar{\omega}_2$ being the more affected at the high velocity levels. It is therefore important that, in describing the performance of a blade, over-all characteristics be used rather than those mass-averaged just at the blade exit. Also, because \bar{e}_2 as well as \bar{e}_1 is independent of the effect of compressibility, these coefficients appear to be more desirable than $\bar{\omega}_1$ and $\bar{\omega}_2$ in describing the blade performance characteristics.

Effect of Trailing-Edge Thickness on Over-All Loss Coefficients

The effect of trailing-edge thickness t/s on the over-all loss coefficients can also be determined through use of the parameter $(t + \delta_{tot})/s$ in figure 4. This effect is best illustrated by an example. The curves of figure 4 were used to compute the over-all loss

coefficients of a blade row having a momentum thickness $\theta^* = 0.01$ and an H^* represented by H corresponding to $n = 0.25$. The results of these calculations are presented in figure 7 in terms of the kinetic-energy-loss coefficient \bar{e}_2 . The ratio of \bar{e}_2 to \bar{e}_2 at zero trailing-edge thickness is plotted as a function of trailing-edge thickness for α_1 of 0° , 30° , and 60° with free-stream critical velocity ratio $(V/V_{cr})_{fs,1}$ as the parameter.

Inspection of figure 7 shows that the trailing-edge thickness, especially at high values, can increase the over-all loss coefficients significantly. For example, at $\alpha_1 = 60^\circ$ and $(V/V_{cr})_{fs,1} = 1.0$, $\bar{e}_2/\bar{e}_{2,t/s=0}$ is 1.25 for a trailing-edge thickness t/s of 0.04. If the thickness is increased to 0.08, $\bar{e}_2/\bar{e}_{2,t/s=0}$ is 1.73.

The effect of compressibility on the trailing-edge loss characteristics can be studied with use of the parameter $(V/V_{cr})_{fs,1}$ in figure 7. For $(V/V_{cr})_{fs,1} \rightarrow 0$, \bar{e}_2 does not vary markedly with angle. For example, at $t/s = 0.04$, $\bar{e}_2/\bar{e}_{2,t/s=0}$ is 1.23 for $\alpha_1 = 0^\circ$ and 1.22 for $\alpha_1 = 60^\circ$. As the flow velocity is increased into the high subsonic and supersonic regions, the trend with compressibility depends on α_1 . At $\alpha_1 = 60^\circ$, the effect of compressibility is small. Again, for $t/s = 0.04$, $\bar{e}_2/\bar{e}_{2,t/s=0}$ increases from 1.22 for incompressible flow to 1.36 for $(V/V_{cr})_{fs,1} = 1.4$. However, at $\alpha_1 = 0^\circ$, a much greater effect can be noted. For $t/s = 0.04$, $\bar{e}_2/\bar{e}_{2,t/s=0}$ increases from 1.23 for incompressible flow to 1.91 for $(V/V_{cr})_{fs,1} = 1.0$. This effect does not extend above $(V/V_{cr})_{fs,1} = 1.0$ because of the limitation imposed by the axial component of the blade-exit Mach number (see fig. 5). Thus, this discussion indicates that increasing the trailing-edge thickness can increase the over-all loss coefficient significantly, with a compressibility effect at low values of α_1 .

SUMMARY OF ANALYSIS

In an analysis to determine the effect of compressibility on the two-dimensional loss characteristics occurring downstream of turbo-machine blade rows, equations were derived for obtaining the compressible-flow boundary-layer characteristics for a simple power velocity profile. Loss coefficients at the blade trailing edge were then obtained in terms of these characteristics. Finally, over-all loss coefficients, which include the effect of mixing downstream of the blade row, were obtained in terms of these characteristics. Pertinent results of the analysis are as follows:

799C

CK-3 back

1. The loss coefficients based on kinetic energy both before and after mixing were approximately independent of compressibility, but the loss coefficients based on pressure were considerably affected. Thus, the loss coefficients based on kinetic energy are the more desirable in describing the compressible-flow blade loss characteristics.

2. The over-all loss coefficients depended directly on the momentum thickness just at the blade trailing edge. Thus, in order to obtain the blade loss characteristics accurately, an accurate evaluation of the momentum thickness must be obtained for compressible-flow conditions, either by experiment or theory.

3. The loss coefficients after mixing were significantly greater than those at the trailing edge, especially at high subsonic and supersonic velocity levels when based on pressure. This effect of mixing should then be included in describing the blade performance characteristics.

4. In the example discussed, increasing the trailing-edge thickness increased the over-all loss coefficients significantly, with an effect of compressibility only at exit flow angles close to axial.

Lewis Flight Propulsion Laboratory
National Advisory Committee for Aeronautics
Cleveland, Ohio, June 8, 1955

199C

APPENDIX A

SYMBOLS

A	parameter equal to $\frac{r-1}{r+1} \left(\frac{v}{v_{cr}} \right)^2$
B	constant equal to $(2\gamma - 1)/(\gamma - 1)$
C	parameter defined in eq. (C16)
D	parameter defined in eq. (C18)
E	energy factor, ψ/θ ; $E^* = \psi^*/\theta^*$
\bar{e}	kinetic-energy-loss coefficient
g	acceleration due to gravity, 32.17 ft/sec ²
H	form factor, δ/θ ; $H^* = \delta^*/\theta^*$
M	Mach number
n	exponent used in describing boundary-layer velocity profile
P	pressure factor, ξ/θ ; $P^* = \xi^*/\theta^*$
p	pressure, lb/sq ft
s	blade spacing, ft
T	temperature, °F abs
t	blade trailing-edge thickness, ft
u	distance in tangential direction, ft
V	gas velocity, ft/sec
w	weight flow, lb/sec
x	distance in axial direction

Y	distance in direction normal to boundary-layer travel, ft
y	distance in direction normal to boundary-layer travel in terms of δ_{full} , $y = Y/\delta_{full}$
α	flow angle measured from axial direction, deg
γ	ratio of specific heats
δ	displacement thickness, ft
δ^*	displacement thickness defined as $\delta_{tot}/s \cos \alpha_1$
δ_{full}	full boundary-layer height, ft
δ_{te}	ratio of tangential component of trailing-edge thickness to spacing, $t/s \cos \alpha_1$
θ	momentum thickness, ft
θ^*	momentum thickness defined as $\theta_{tot}/s \cos \alpha_1$
ξ	pressure thickness, ft
ξ^*	pressure thickness defined as $\xi_{tot}/s \cos \alpha_1$
ρ	gas density, lb/cu ft
ψ	energy thickness, ft
ψ^*	energy thickness defined as $\psi_{tot}/s \cos \alpha_1$
\bar{w}	pressure-loss coefficient

Subscripts:

cr	conditions at Mach number of 1
fs	conditions at free-stream or that region between blade wakes
p	pressure surface
s	suction surface
th	theoretical

tot sum of suction and pressure surface quantities

u tangential component

x axial component

0 station upstream of blade row

1 station just downstream of blade row

2 station after complete mixing occurs

Superscripts:

' total state

- refers to mass-averaged quantity

3667

APPENDIX B

DEVELOPMENT OF EQUATIONS FOR FORM, ENERGY, AND PRESSURE

FACTORS IN TERMS OF COMPRESSIBLE FLOW

This appendix presents the development of the equations used in obtaining the form factor H , energy factor E , and pressure factor P in terms of compressible flow. The equations for these parameters are

$$H = \frac{1 - \int_0^1 \frac{\rho V}{\rho_{fs} V_{fs}} dy}{\int_0^1 \frac{\rho V}{\rho_{fs} V_{fs}} dy - \int_0^1 \frac{\rho V^2}{\rho_{fs} V_{fs}^2} dy} \quad (7)$$

$$E = \frac{\int_0^1 \frac{\rho V}{\rho_{fs} V_{fs}} dy - \int_0^1 \frac{\rho V^3}{\rho_{fs} V_{fs}^3} dy}{\int_0^1 \frac{\rho V}{\rho_{fs} V_{fs}} dy - \int_0^1 \frac{\rho V^2}{\rho_{fs} V_{fs}^2} dy} \quad (9)$$

and

$$P = \frac{\int_0^1 \frac{\rho V}{\rho_{fs} V_{fs}} dy - \int_0^1 \frac{p'}{p'_{fs}} \frac{\rho V}{\rho_{fs} V_{fs}} dy}{\left[1 - \left(\frac{p}{p'} \right)_{fs} \right] \left(\int_0^1 \frac{\rho V}{\rho_{fs} V_{fs}} dy - \int_0^1 \frac{\rho V^2}{\rho_{fs} V_{fs}^2} dy \right)} \quad (11)$$

In order to perform the necessary integrations for the simple power velocity profile

$$\frac{V}{V_{fs}} = y^n \quad (12)$$

equations (7), (9), and (11) must be expressed in terms of V/V_{fs} so that equation (12) can be used. With the assumptions that the total temperature and static pressure are constant within the boundary layer and equal to the free-stream values,

$$\frac{\rho}{\rho_{fs}} = \frac{\frac{T_{fs}}{T'}}{\frac{T}{T'}} \quad (B1)$$

and

$$\frac{p'}{p_{fs}} = \frac{\frac{p}{p_{fs}}}{\frac{p}{p'}} = \frac{\left(\frac{T_{fs}}{T'}\right)^{\frac{\gamma}{\gamma-1}}}{\left(\frac{T}{T'}\right)^{\frac{\gamma}{\gamma-1}}} \quad (B2)$$

The energy equation can be written

$$\begin{aligned} \frac{T}{T'} &= 1 - \frac{\gamma-1}{\gamma+1} \left(\frac{V}{V_{cr}}\right)^2 \\ &= 1 - A \end{aligned} \quad (B3)$$

where

$$A \equiv \frac{\gamma-1}{\gamma+1} \left(\frac{V}{V_{cr}}\right)^2 \quad (B4)$$

Thus, substituting equations (B4) and (B3) into (B1) and (B2),

$$\frac{\rho}{\rho_{fs}} = (1 - A_{fs})(1 - A)^{-1} \quad (B5)$$

and

$$\frac{p'}{p_{fs}} = (1 - A_{fs})^{\frac{\gamma}{\gamma-1}} (1 - A)^{-\frac{\gamma}{\gamma-1}} \quad (B6)$$

Finally, substituting equations (B5), (B6), and (12) into equations (7), (9), and (11) and noting that $A = A_{fs} y^{2n}$,

$$H = \frac{\frac{1}{1 - A_{fs}} - \int_0^1 (1 - A_{fs} y^{2n})^{-1} y^n dy}{\int_0^1 (1 - A_{fs} y^{2n})^{-1} y^n dy - \int_0^1 (1 - A_{fs} y^{2n})^{-1} y^{2n} dy} \quad (B7)$$

$$E = \frac{\int_0^1 (1 - A_{fs} y^{2n})^{-1} y^n dy - \int_0^1 (1 - A_{fs} y^{2n})^{-1} y^{3n} dy}{\int_0^1 (1 - A_{fs} y^{2n})^{-1} y^n dy - \int_0^1 (1 - A_{fs} y^{2n})^{-1} y^{2n} dy} \quad (B8)$$

and

$$P = \frac{\int_0^1 (1 - A_{fs} y^{2n})^{-1} y^n dy - (1 - A_{fs})^{\frac{\gamma}{\gamma-1}} \int_0^1 (1 - A_{fs} y^{2n})^{-\frac{2\gamma-1}{\gamma-1}} y^n dy}{\left[\int_0^1 (1 - A_{fs} y^{2n})^{-1} y^n dy - \int_0^1 (1 - A_{fs} y^{2n})^{-1} y^{2n} dy \right] \left[1 - \left(\frac{p}{p_i} \right)_{fs} \right]} \quad (B9)$$

The individual integrations were performed using the binominal expansion to yield

$$\int_0^1 (1 - A_{fs} y^{2n})^{-1} y^n dy = \frac{1}{n+1} + \frac{A_{fs}}{3n+1} + \frac{A_{fs}^2}{5n+1} + \dots$$

$$\int_0^1 (1 - A_{fs} y^{2n})^{-1} y^{2n} dy = \frac{1}{2n+1} + \frac{A_{fs}}{4n+1} + \frac{A_{fs}^2}{6n+1} + \dots$$

$$\int_0^1 (1 - A_{fs} y^{2n})^{-1} y^{3n} dy = \frac{1}{3n+1} + \frac{A_{fs}}{5n+1} + \frac{A_{fs}^2}{7n+1} + \dots$$

and

$$\int_0^1 (1 - A_{fs} y^{2n})^{-\frac{2\gamma-1}{\gamma-1}} y^n dy = \frac{1}{n+1} + \frac{BA_{fs}}{3n+1} + \frac{B(B+1)}{2!} \frac{A_{fs}^2}{5n+1} + \dots$$

(B10)

where $B = (2\gamma - 1)/(\gamma - 1)$.

Also,

$$\frac{1}{1 - A_{fs}} = 1 + A_{fs} + A_{fs}^2 + A_{fs}^3 + \dots \quad (B11)$$

So, substituting (B10) and (B11) into equations (B7), (B8), and (B9) and combining where desired yield

$$H = \frac{\frac{1}{n+1} + \frac{3A_{fs}}{3n+1} + \frac{5A_{fs}^2}{5n+1} + \dots}{\frac{1}{(n+1)(2n+1)} + \frac{A_{fs}}{(3n+1)(4n+1)} + \frac{A_{fs}^2}{(5n+1)(6n+1)} + \dots}$$

(B12)

$$E = \frac{2 \left[\frac{1}{(n+1)(3n+1)} + \frac{A_{fs}}{(3n+1)(5n+1)} + \frac{A_{fs}^2}{(5n+1)(7n+1)} + \dots \right]}{\frac{1}{(n+1)(2n+1)} + \frac{A_{fs}}{(3n+1)(4n+1)} + \frac{A_{fs}^2}{(5n+1)(6n+1)} + \dots} \quad (B13)$$

$$P = \frac{\frac{1 - \left(\frac{p}{p_i}\right)_{fs}}{n+1} + \frac{A_{fs} \left[1 - \left(\frac{p}{p_i}\right)_{fs} B \right]}{3n+1} + \frac{A_{fs}^2 \left[1 - \left(\frac{p}{p_i}\right)_{fs} \frac{B(B+1)}{2!} \right]}{5n+1} + \dots}{n \left[1 - \left(\frac{p}{p_i}\right)_{fs} \right] \left[\frac{1}{(n+1)(2n+1)} + \frac{A_{fs}}{(3n+1)(4n+1)} + \frac{A_{fs}^2}{(5n+1)(6n+1)} + \dots \right]} \quad (B14)$$

where

$$\left(\frac{p}{p_i}\right)_{fs} = (1 - A_{fs})^{\frac{\gamma}{\gamma-1}}$$

As $(V/V_{cr})_{fs} \rightarrow 0$, H and E can easily be obtained from equations (B12) and (B13). The limit on P as $(V/V_{cr})_{fs} \rightarrow 0$ cannot be determined directly from equation (B14). However, it can be shown that $P \left(\frac{V}{V_{cr}}\right)_{fs,1} \rightarrow 0 = E \left(\frac{V}{V_{cr}}\right)_{fs,1} \rightarrow 0$. Thus, from equations (B12) to (B14) the expressions

$$H \left(\frac{V}{V_{cr}}\right)_{fs} \rightarrow 0 = 2n + 1 \quad (B15)$$

$$P \left(\frac{V}{V_{cr}}\right)_{fs} \rightarrow 0 = E \left(\frac{V}{V_{cr}}\right)_{fs} \rightarrow 0 = \frac{2(2n+1)}{3n+1} \quad (B16)$$

are obtained. These expressions are the same as those obtained considering air incompressible.

It is also desired that the limits in the parameters as $n \rightarrow 0$ be obtained. These limits can again be derived directly from equations

(B12) and (B13) for H and E but must be obtained from (B14) using L'Hospital's rule. Thus,

$$\lim_{n \rightarrow 0} H = \frac{1 + A_{fs}}{1 - A_{fs}} \quad (B17)$$

$$\lim_{n \rightarrow 0} E = 2 \quad (B18)$$

$$\lim_{n \rightarrow 0} P = 2 \left[\frac{\frac{\gamma}{\gamma - 1} A_{fs}}{(1 - A_{fs}) - (1 - A_{fs})^{\frac{2\gamma-1}{\gamma-1}}} \right] \quad (B19)$$

These limits might have been obtained directly from the basic equations (6), (8), and (10) by letting $V/V_{fs} \rightarrow 1$ and using L'Hospital's rule.

APPENDIX C

DERIVATION OF EQUATIONS USED TO OBTAIN OVER-ALL LOSS COEFFICIENTS

IN TERMS OF BASIC BOUNDARY-LAYER CHARACTERISTICS

The equations used to obtain the kinetic-energy-loss coefficient \bar{e}_2 and the pressure-loss coefficient \bar{w}_2 in terms of the basic boundary-layer characteristics at station 1 are derived herein. The basic equations are described, and solutions for incompressible and compressible flows are given.

Basic Equations

The following equations are used to relate conditions between stations 1 and 2:

Continuity. - At station 1

$$w = \cos \alpha_1 \int_0^1 (\rho V)_1 d\left(\frac{u}{s}\right)$$

and at station 2

$$w = (\rho V)_2 \cos \alpha_2$$

Equating weight flows at stations 1 and 2 gives

$$\cos \alpha_1 \int_0^1 (\rho V)_1 d\left(\frac{u}{s}\right) = \cos \alpha_2 (\rho V)_2$$

or, using equation (17a),

$$\cos \alpha_1 (1 - \delta^* - \delta_{te})(\rho V)_{fs,1} = \cos \alpha_2 (\rho V)_2 \quad (C1)$$

Momentum in tangential direction. - The following equation relates the tangential momentum at stations 1 and 2:

$$\sin \alpha_1 \cos \alpha_1 \int_0^1 (\rho V^2)_1 d\left(\frac{u}{s}\right) = \sin \alpha_2 \cos \alpha_2 (\rho V^2)_2$$

Using equations (17a) and (17b),

$$\sin \alpha_1 \cos \alpha_1 (1 - \delta^* - \delta_{te} - \theta^*)(\rho V^2)_{fs,1} = \sin \alpha_2 \cos \alpha_2 (\rho V^2)_2 \quad (C2)$$

Momentum in axial direction. - The equation used in conserving momentum in the axial direction is more complicated than that in the tangential direction, in that change in static pressure must be considered. This equation is

$$g p_1 + \cos^2 \alpha_1 \int_0^1 (\rho V^2)_1 d\left(\frac{u}{s}\right) = g p_2 + \cos^2 \alpha_2 (\rho V^2)_2$$

Again using equations (17a) and (17b),

$$g p_1 + \cos^2 \alpha_1 (1 - \delta^* - \delta_{te} - \theta^*)(\rho V^2)_{fs,1} = g p_2 + \cos^2 \alpha_2 (\rho V^2)_2 \quad (C3)$$

Incompressible-Flow Solution

The incompressible-flow case can be said to represent the lower limit to the compressible-flow case where $(V/V_{cr})_{fs,1} \rightarrow 0$. For this case the density is specified constant. Thus, the over-all pressure-loss coefficient $\bar{w}_2, \left(\frac{V}{V_{cr}}\right)_{fs,1} \rightarrow 0$ is equal to $\bar{e}_2, \left(\frac{V}{V_{cr}}\right)_{fs,1} \rightarrow 0$ and can be written

as

$$\bar{w}_2, \left(\frac{V}{V_{cr}}\right)_{fs,1} \rightarrow 0 = \bar{e}_2, \left(\frac{V}{V_{cr}}\right)_{fs,1} \rightarrow 0 = \frac{p_0' - p_2'}{p_0' - p_2}$$

Now, for incompressible flow

$$p_0' = p_1 + \frac{1}{2g} (\rho V^2)_{fs,1} \quad \text{and} \quad p_2' = p_2 + \frac{1}{2g} (\rho V^2)_2$$

so $\bar{\omega}_2$ can be written as

$$\bar{\omega}_2, \left(\frac{V}{V_{cr}}\right)_{fs,1} \rightarrow 0 = 1 - \frac{\left(\frac{V_2}{V_{fs,1}}\right)^2}{1 + \frac{P_1 - P_2}{\frac{1}{2g} (\rho V^2)_{fs,1}}} \quad (C4)$$

It is desired to use the basic equations (C1) to (C3) in order that $\bar{\omega}_2$ can be expressed in terms of conditions at station 1 only.

Rewriting equation (C3) gives

$$P_1 - P_2 = \cos^2 \alpha_2 \frac{(\rho V)_2^2}{g} - \cos^2 \alpha_1 \frac{(\rho V^2)_{fs,1}}{g} (1 - \delta^* - \delta_{te} - \theta^*)$$

or

$$\frac{P_1 - P_2}{\frac{1}{2g} (\rho V^2)_{fs,1}} = 2 \cos^2 \alpha_2 \left(\frac{V_2}{V_{fs,1}}\right)^2 - 2 \cos^2 \alpha_1 (1 - \delta^* - \delta_{te} - \theta^*) \quad (C5)$$

Also, rearranging equation (C1) and squaring yield

$$\cos^2 \alpha_2 \left(\frac{V_2}{V_{fs,1}}\right)^2 = \cos^2 \alpha_1 (1 - \delta^* - \delta_{te})^2$$

Substituting into (C5),

$$\frac{P_1 - P_2}{\frac{1}{2g} (\rho V^2)_{fs,1}} = 2 \cos^2 \alpha_1 \left[(1 - \delta^* - \delta_{te})^2 - (1 - \delta^* - \delta_{te} - \theta^*) \right] \quad (C6)$$

Equations (C1) and (C2) are now solved for $(V_2/V_{fs,1})^2$ in terms of conditions at station 1:

$$\left(\frac{V_2}{V_{fs,1}}\right)^2 = \frac{\cos^2 \alpha_1}{\cos^2 \alpha_2} (1 - \delta^* - \delta_{te})^2 \quad (C7)$$

$$\left(\frac{V_2}{V_{fs,1}}\right)^2 = \frac{\sin \alpha_1 \cos \alpha_1}{\sin \alpha_2 \cos \alpha_2} (1 - \delta^* - \delta_{te} - \theta^*) \quad (C8)$$

Equating (C7) and (C8) gives

$$\frac{\cos \alpha_1}{\cos \alpha_2} (1 - \delta^* - \delta_{te})^2 = \frac{\sin \alpha_1}{\sin \alpha_2} (1 - \delta^* - \delta_{te} - \theta^*)$$

Squaring and using trigonometry,

$$\frac{\cos^2 \alpha_1}{\cos^2 \alpha_2} (1 - \delta^* - \delta_{te})^4 = \frac{\sin^2 \alpha_1}{1 - \cos^2 \alpha_2} (1 - \delta^* - \delta_{te} - \theta^*)^2$$

and solving for $\cos^2 \alpha_1 / \cos^2 \alpha_2$,

$$\frac{\cos^2 \alpha_1}{\cos^2 \alpha_2} = \sin^2 \alpha_1 \frac{(1 - \delta^* - \delta_{te} - \theta^*)^2}{(1 - \delta^* - \delta_{te})^4} + \cos^2 \alpha_1 \quad (C9)$$

Substituting equation (C9) into equation (C7) gives

$$\left(\frac{V_2}{V_{fs,1}}\right)^2 = \sin^2 \alpha_1 \frac{(1 - \delta^* - \delta_{te} - \theta^*)^2}{(1 - \delta^* - \delta_{te})^2} + \cos^2 \alpha_1 (1 - \delta^* - \delta_{te})^2 \quad (C10)$$

Finally, substituting equations (C6) and (C10) in equation (C4) gives

$$\bar{\omega}_2, \left(\frac{V}{V_{cr}}\right)_{fs,1} \rightarrow 0 = 1 - \frac{\sin^2 \alpha_1 \frac{(1 - \delta^* - \delta_{te} - \theta^*)^2}{(1 - \delta^* - \delta_{te})^2} + \cos^2 \alpha_1 (1 - \delta^* - \delta_{te})^2}{1 + 2 \cos^2 \alpha_1 [(1 - \delta^* - \delta_{te})^2 - (1 - \delta^* - \delta_{te} - \theta^*)^2]} \quad (C11)$$

where

$$\delta_{te} + \delta^* = \frac{t + \delta_{tot}}{s \cos \alpha_1}$$

3667

5-CK

Equation (C11) was used to obtain $\bar{\omega}_2 = \bar{e}_2$ for $(V/V_{cr})_{fs,1} \rightarrow 0$ and is graphically shown in figure 4(a).

Compressible-Flow Solution

In the compressible-flow solution the density ρ is not constant and must be included as a variable in the equations. So, for this solution, equations (C1) to (C3) are written in dimensionless form as

$$\cos \alpha_1 (1 - \delta^* - \delta_{te}) \left(\frac{\rho V}{\rho' V_{cr}} \right)_{fs,1} = \left(\frac{\rho V_x}{\rho' V_{cr}} \right)_2 \frac{p_2'}{p_0'} \quad (C12)$$

$$\sin \alpha_1 \cos \alpha_1 (1 - \delta^* - \delta_{te} - \theta^*) \left(\frac{\rho V^2}{\rho' V_{cr}^2} \right)_{fs,1} = \left(\frac{\rho V_x V_u}{\rho' V_{cr}^2} \right)_2 \frac{p_2'}{p_0'} \quad (C13)$$

$$\begin{aligned} \frac{p_1}{p_0'} \left(\frac{\gamma + 1}{2\gamma} \right) + \cos^2 \alpha_1 (1 - \delta^* - \delta_{te} - \theta^*) \left(\frac{\rho V^2}{\rho' V_{cr}^2} \right)_{fs,1} \\ = \frac{p_2}{p_2'} \frac{p_2'}{p_0'} \left(\frac{\gamma + 1}{2\gamma} \right) + \left(\frac{\rho V_x^2}{\rho' V_{cr}^2} \right)_2 \frac{p_2'}{p_0'} \end{aligned} \quad (C14)$$

Solving (C12) for p_2'/p_0' and substituting into (C14) with $p_1/p_0' = (\rho/\rho')_{fs,1} (1 - A_{fs,1})$ yield

$$\begin{aligned} (1 - A_{fs,1}) \frac{\gamma + 1}{2\gamma} + \cos^2 \alpha_1 (1 - \delta^* - \delta_{te} - \theta^*) \left(\frac{V}{V_{cr}} \right)_{fs,1}^2 \\ = \left[\frac{p_2}{p_2'} \frac{\gamma + 1}{2\gamma} + \left(\frac{\rho V_x^2}{\rho' V_{cr}^2} \right)_2 \right] \left[\frac{\cos \alpha_1 (1 - \delta^* - \delta_{te}) \left(\frac{V}{V_{cr}} \right)_{fs,1}}{\left(\frac{\rho V_x}{\rho' V_{cr}} \right)_2} \right] \end{aligned} \quad (C15)$$

or, defining

$$C \equiv \frac{(1 - A_{fs,1}) \frac{\gamma + 1}{2\gamma} + \cos^2 \alpha_1 (1 - \delta^* - \delta_{te} - \theta^*) \left(\frac{V}{V_{cr}} \right)_{fs,1}^2}{\cos \alpha_1 (1 - \delta^* - \delta_{te}) \left(\frac{V}{V_{cr}} \right)_{fs,1}} \quad (C16)$$

equation (C15) becomes

$$\left(\frac{\rho V_x^2}{\rho' V_{cr}^2}\right)_2 - C \left(\frac{\rho V_x}{\rho' V_{cr}}\right)_2 + \frac{\gamma + 1}{2\gamma} \frac{p_2}{p_2'} = 0$$

Using the equations of state and energy, this equation reduces to

$$\left(\frac{V_x}{V_{cr}}\right)_2^2 - C \left(\frac{V_x}{V_{cr}}\right)_2 + \frac{\gamma + 1}{2\gamma} \left\{ 1 - \frac{\gamma - 1}{\gamma + 1} \left[\left(\frac{V_x}{V_{cr}}\right)_2^2 + \left(\frac{V_u}{V_{cr}}\right)_2^2 \right] \right\} = 0 \quad (C17)$$

Now, solving equations (C12) and (C13) for $(V_u/V_{cr})_2$,

$$\left(\frac{V_u}{V_{cr}}\right)_2 \equiv D = \left(\frac{V}{V_{cr}}\right)_{fs,1} \sin \alpha_1 \left(\frac{1 - \delta^* - \delta_{te} - \theta^*}{1 - \delta^* - \delta_{te}} \right) \quad (C18)$$

Equation (C17) can thus be expressed in terms of $(V_x/V_{cr})_2$ using equation (C18) as

$$\left(\frac{V_x}{V_{cr}}\right)_2^2 - \frac{2\gamma C}{\gamma + 1} \left(\frac{V_x}{V_{cr}}\right)_2 + \left(1 - \frac{\gamma - 1}{\gamma + 1} D^2\right) = 0 \quad (C19)$$

The terms C and D are known, as they are functions of station 1 only. Equation (C19) is a quadratic equation in $(V_x/V_{cr})_2$ with the solution

$$\left(\frac{V_x}{V_{cr}}\right)_2 = \frac{\gamma C}{\gamma + 1} - \sqrt{\left(\frac{\gamma C}{\gamma + 1}\right)^2 - 1 + \frac{\gamma - 1}{\gamma + 1} D^2} \quad (C20)$$

The minus sign is used in this solution to yield the correct conditions after mixing. Once $(V_x/V_{cr})_2$ is obtained from equation (C20), the density ratio $(\rho/\rho')_2$ is obtained from

$$\left(\frac{\rho}{\rho'}\right)_2 = \left\{ 1 - \frac{\gamma - 1}{\gamma + 1} \left[D^2 + \left(\frac{V_x}{V_{cr}}\right)_2^2 \right] \right\}^{\frac{1}{\gamma - 1}} \quad (C21)$$

3667

CK-5 back

Equation (C12) can then be solved for p_2'/p_0' as

$$\frac{p_2'}{p_0'} = \frac{\left(\frac{\rho V}{\rho' V_{cr}}\right)_{fs,1} \cos \alpha_1 (1 - \delta^* - \delta_{te})}{\left(\frac{\rho V_x}{\rho' V_{cr}}\right)_2} \quad (C22)$$

Now, for the compressible-flow case \bar{e}_2 and $\bar{\omega}_2$ are expressed as

$$\bar{e}_2 = \frac{\frac{\gamma-1}{\left(\frac{p_0'}{p_2'}\right)^\gamma - 1}}{\frac{\gamma-1}{\left(\frac{p_0'}{p_2'}\right)^\gamma - 1}} \quad (24)$$

and

$$\bar{\omega}_2 = \frac{1 - \frac{p_2'}{p_0'}}{1 - \frac{p_2}{p_0'}} \quad (25)$$

Thus, in solving for \bar{e}_2 and $\bar{\omega}_2$ the following steps are needed:

(1) For specified conditions at station 1, the parameters C and D can be computed from equations (C16) and (C18).

(2) $(V_x/V_{cr})_2$ can be computed from equation (C20).

(3) $(\rho/\rho')_2$ can be obtained from equation (C21).

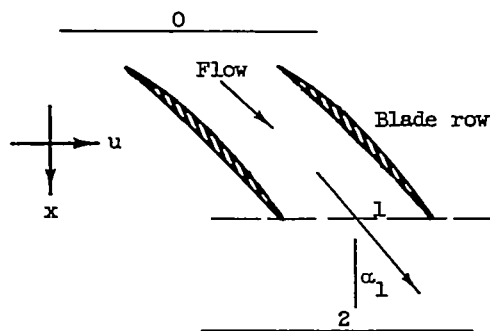
(4) p_2'/p_0' can be computed from equation (C22).

(5) $(p/p')_2$ can be computed from step (3) and the relation $(p/p')_2 = (\rho/\rho')_2^\gamma$.

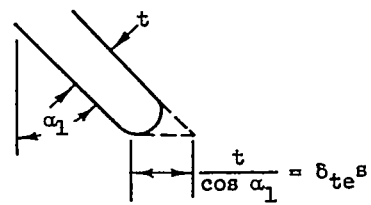
(6) Finally, \bar{e}_2 and $\bar{\omega}_2$ can be obtained from equations (24) and (25).

With these equations, figures 4(b) to (e) are obtained in a form similar to figure 4(a).

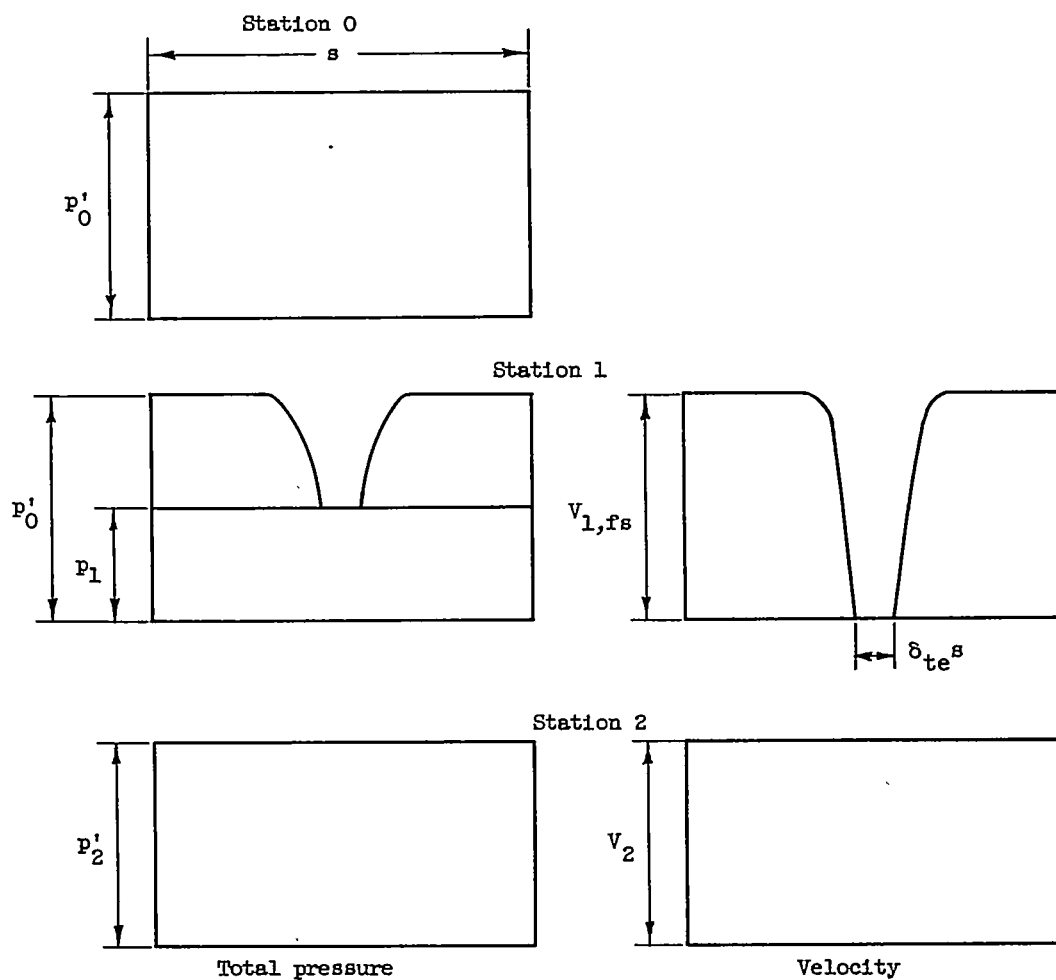
When the equations just described are used for $(V/V_{cr})_{fs,1} > 1$, an oblique shock solution occurs at certain values of α_1 . Physically, this solution occurs when the axial component of the Mach number at station 1 is greater than unity: that is, if $M_{fs,1} \cos \alpha_1 > 1$. Thus, in the supersonic solution a limit of $M_{fs,1} = 1/\cos \alpha_1$ was used. This limiting angle is presented in figure 5 as a function of $(V/V_{cr})_{fs,1}$ and is used in figures 4(d) and (e).



(a) Station nomenclature.



(b) Enlargement of blade trailing edge.



(c) Total-pressure and velocity distributions.

Figure 1. - Description of total-pressure and velocity distributions used in analysis.

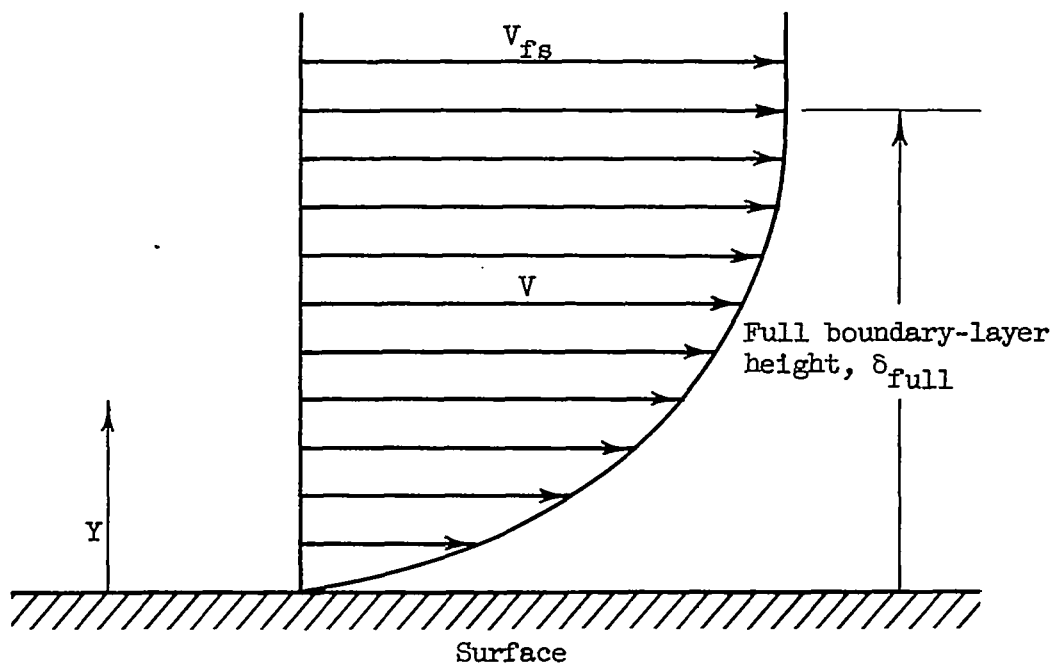
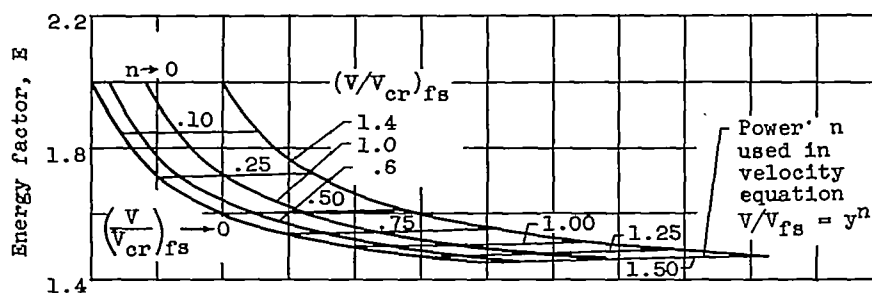
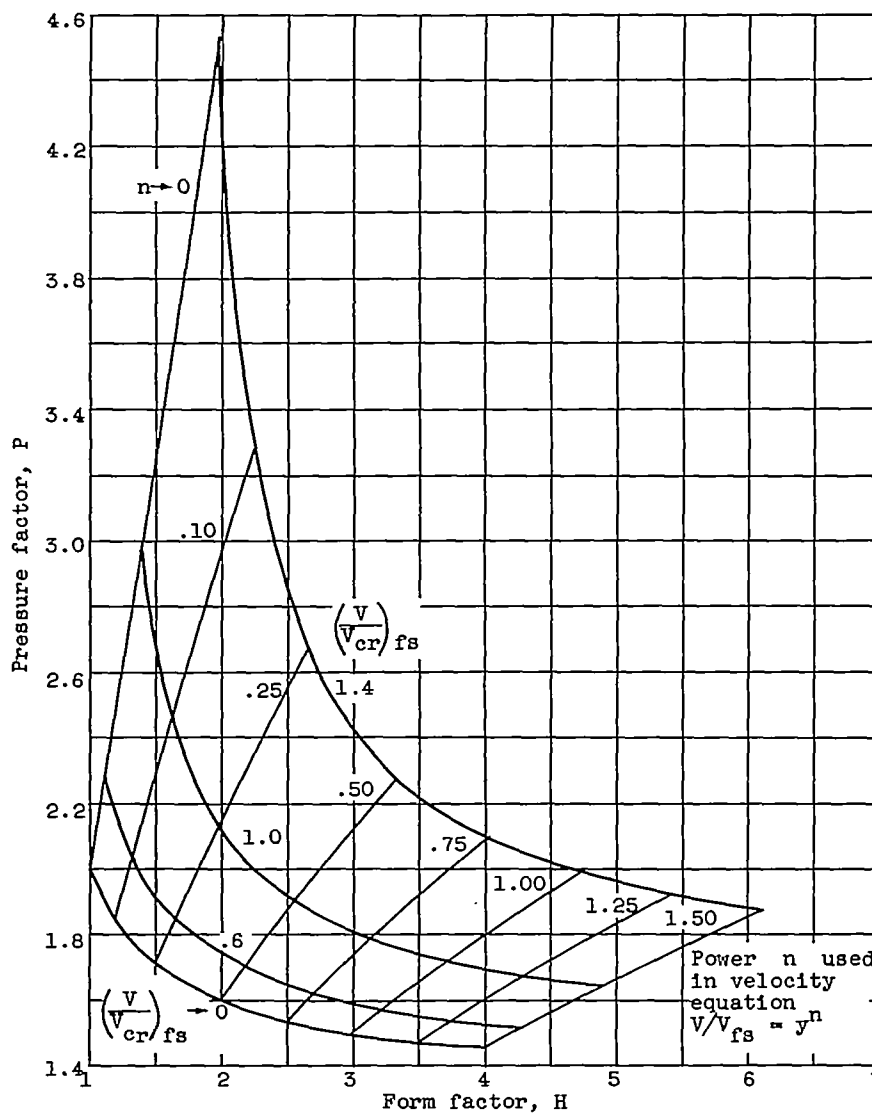


Figure 2. - Typical boundary-layer velocity profile.



(a) Energy factor.



(b) Pressure factor.

Figure 3. - Effect of compressibility on variation of energy and pressure factors with form factor for simple power boundary layer.

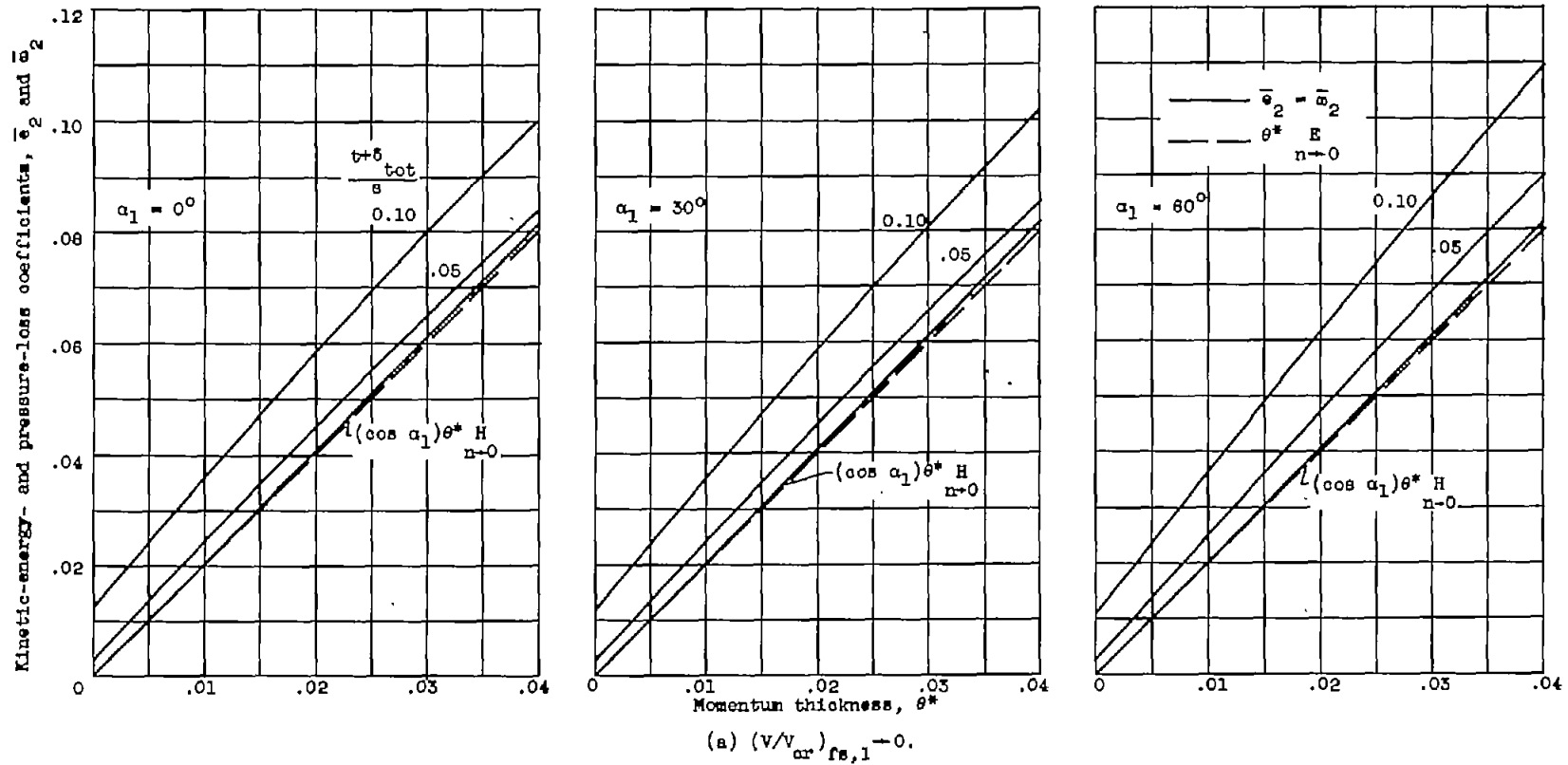
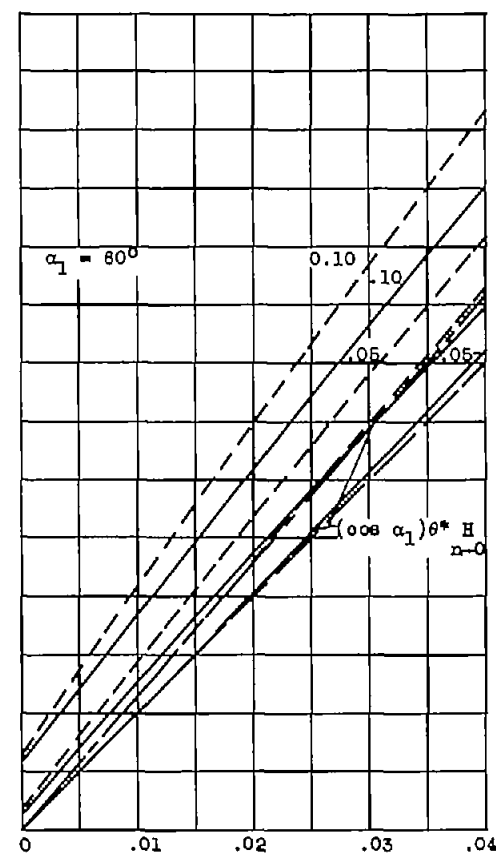
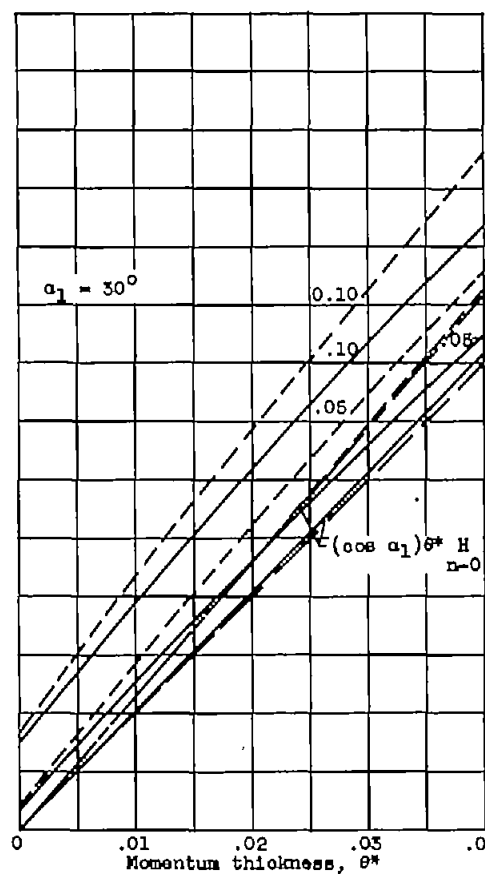
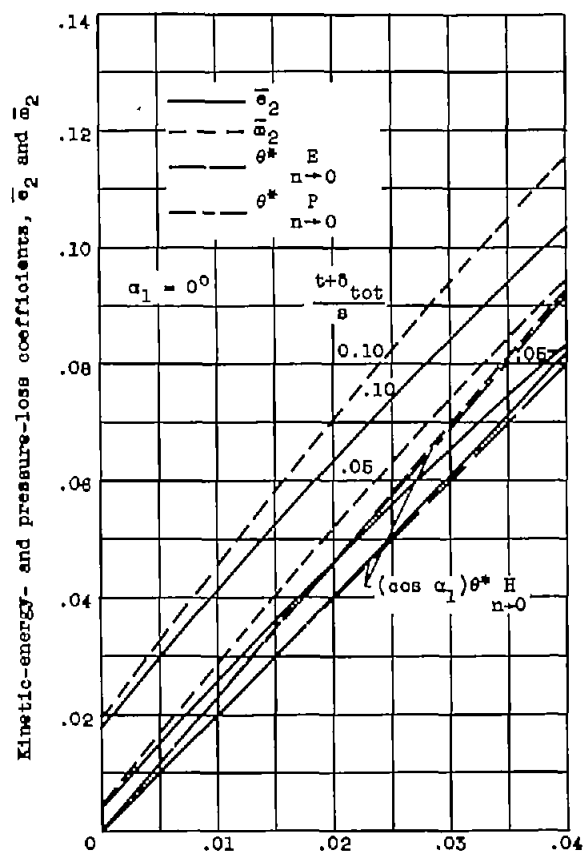
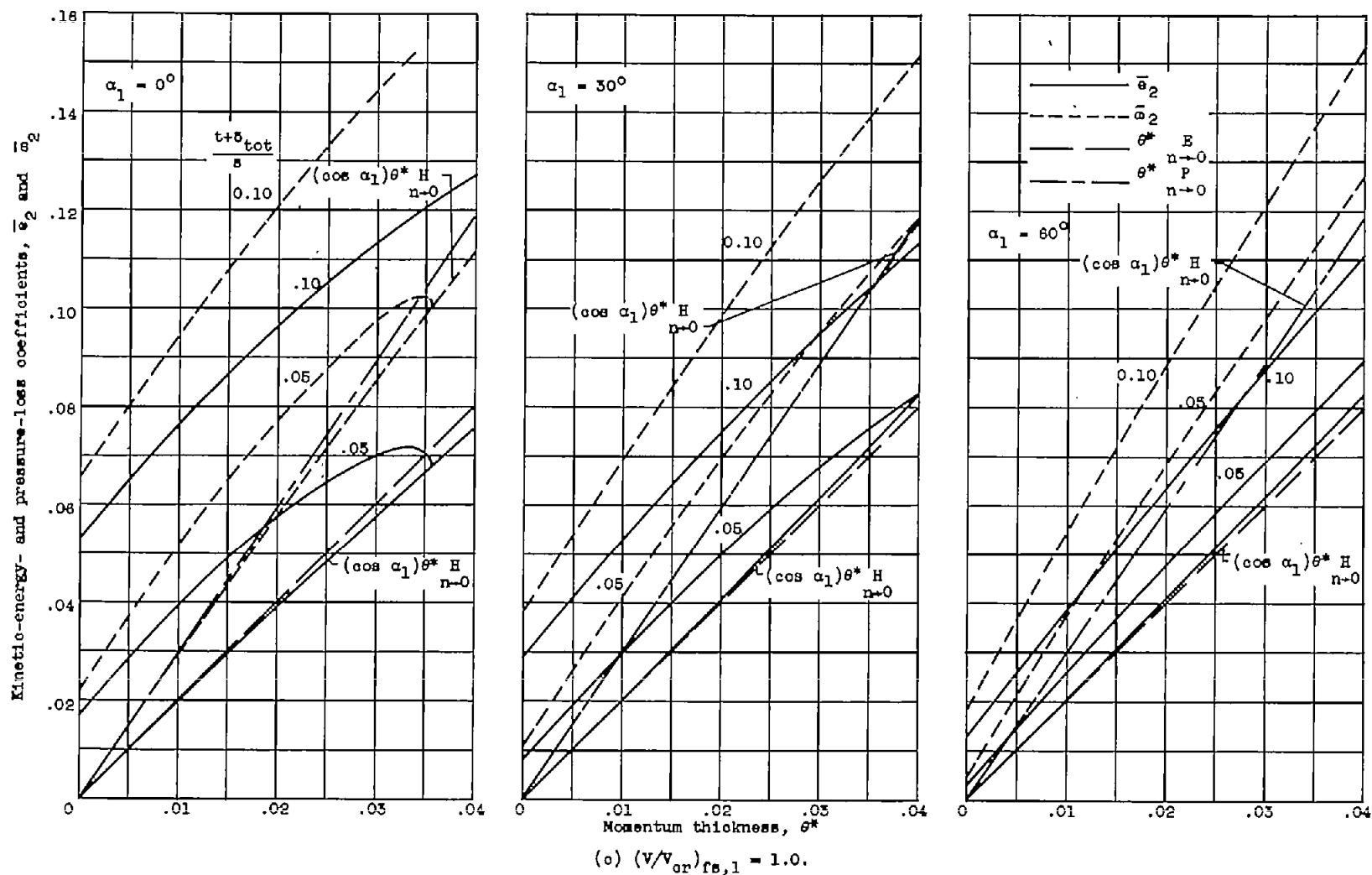


Figure 4. - Blade loss characteristics.



(b) $(V/V_{ar})_{fs,1} = 0.6$.

Figure 4. - Continued. Blade loss characteristics.



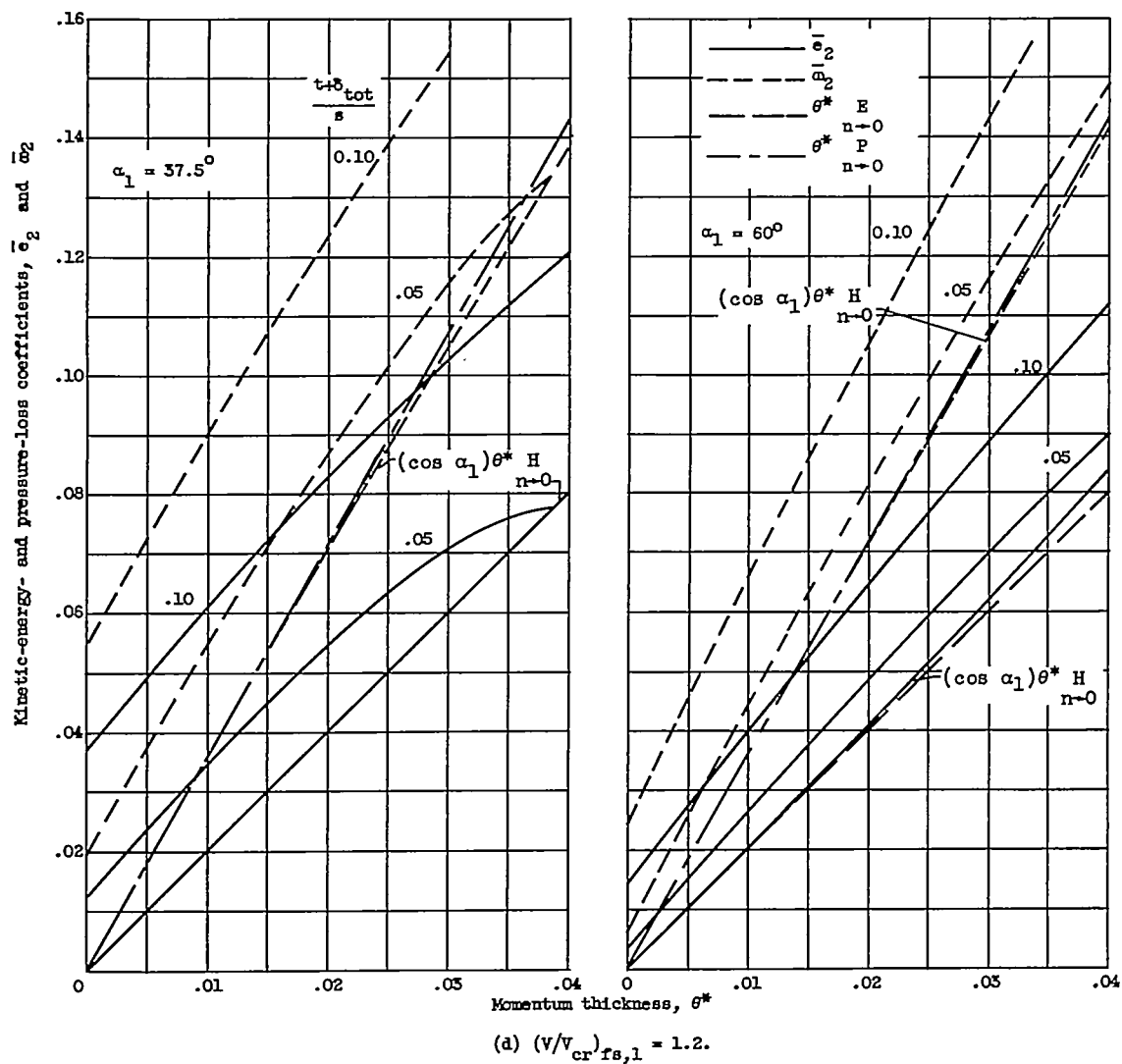


Figure 4. - Continued. Blade loss characteristics.

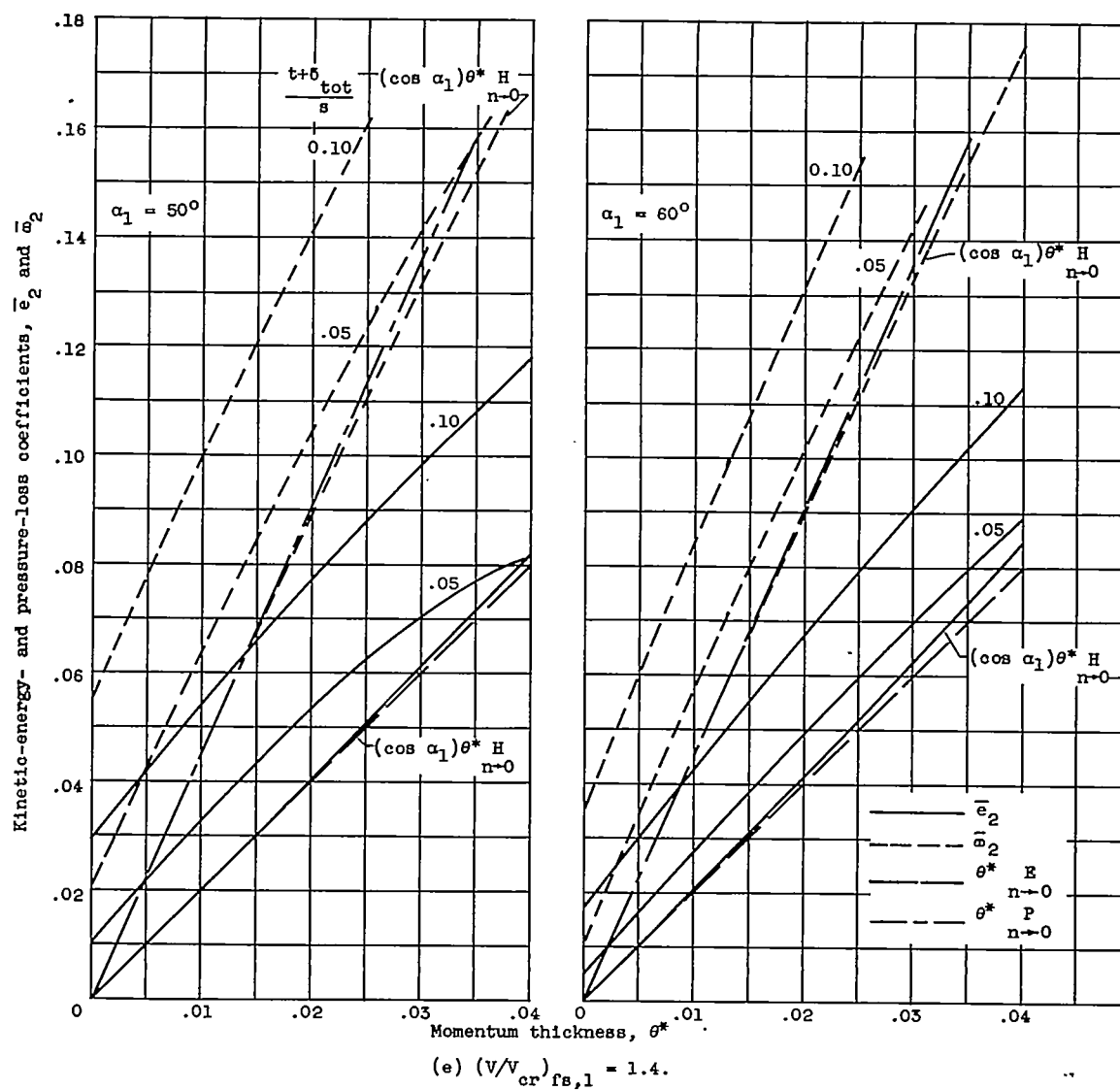


Figure 4. - Concluded. Blade loss characteristics.

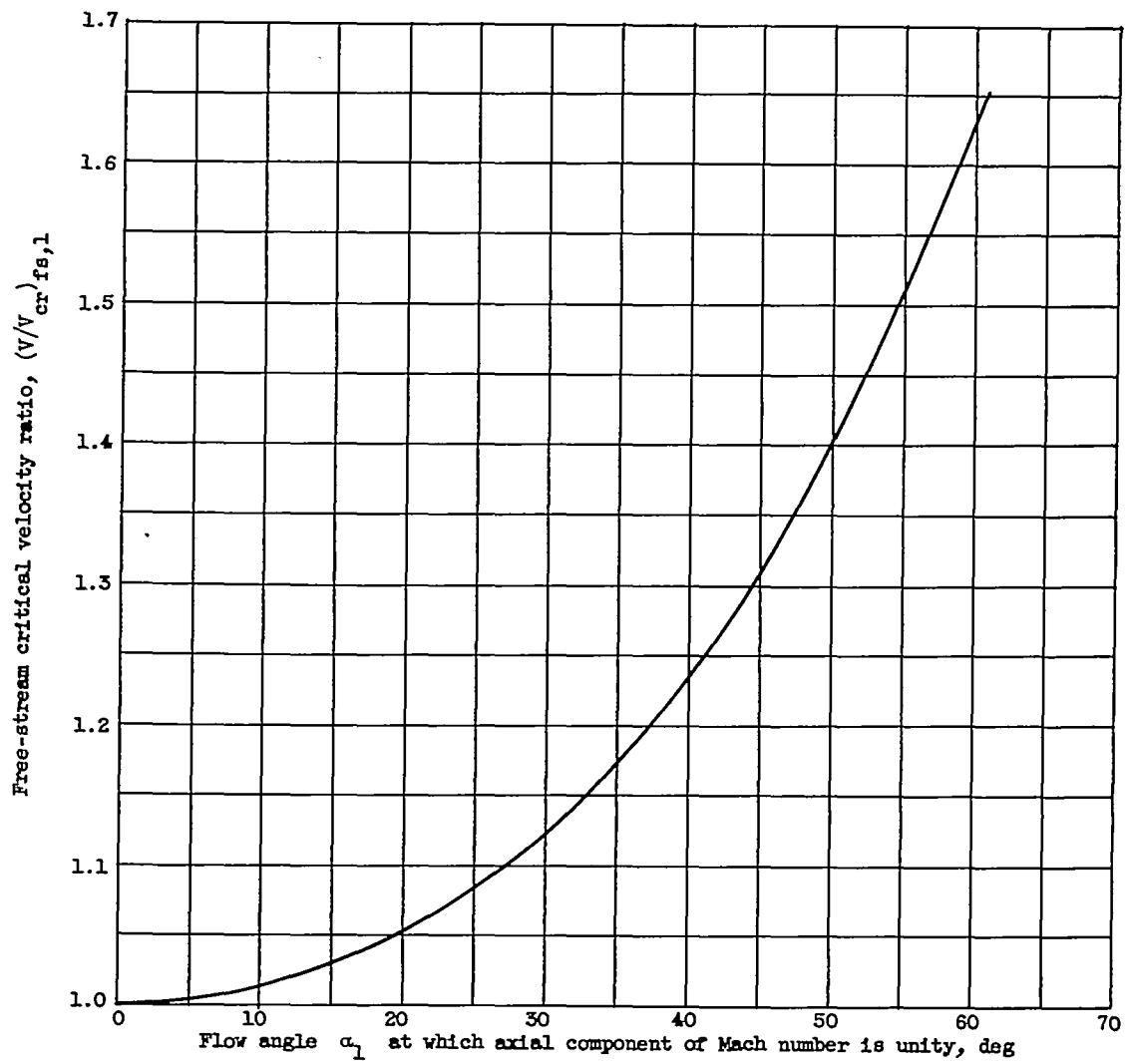


Figure 5. - Variation of free-stream critical velocity ratio with angle at which axial component of Mach number is unity.

3657

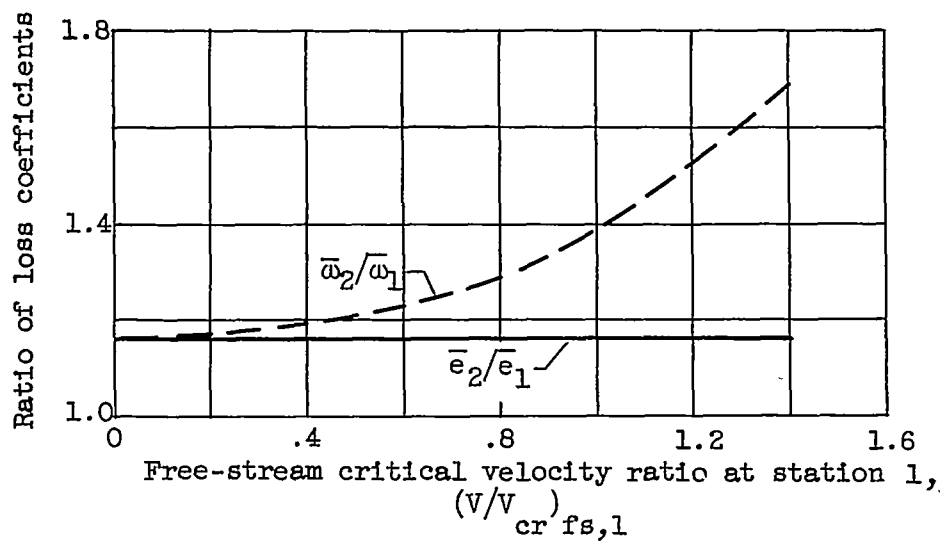


Figure 6. - Effect of compressibility on blade mixing-loss characteristics for $n = 0.25$.

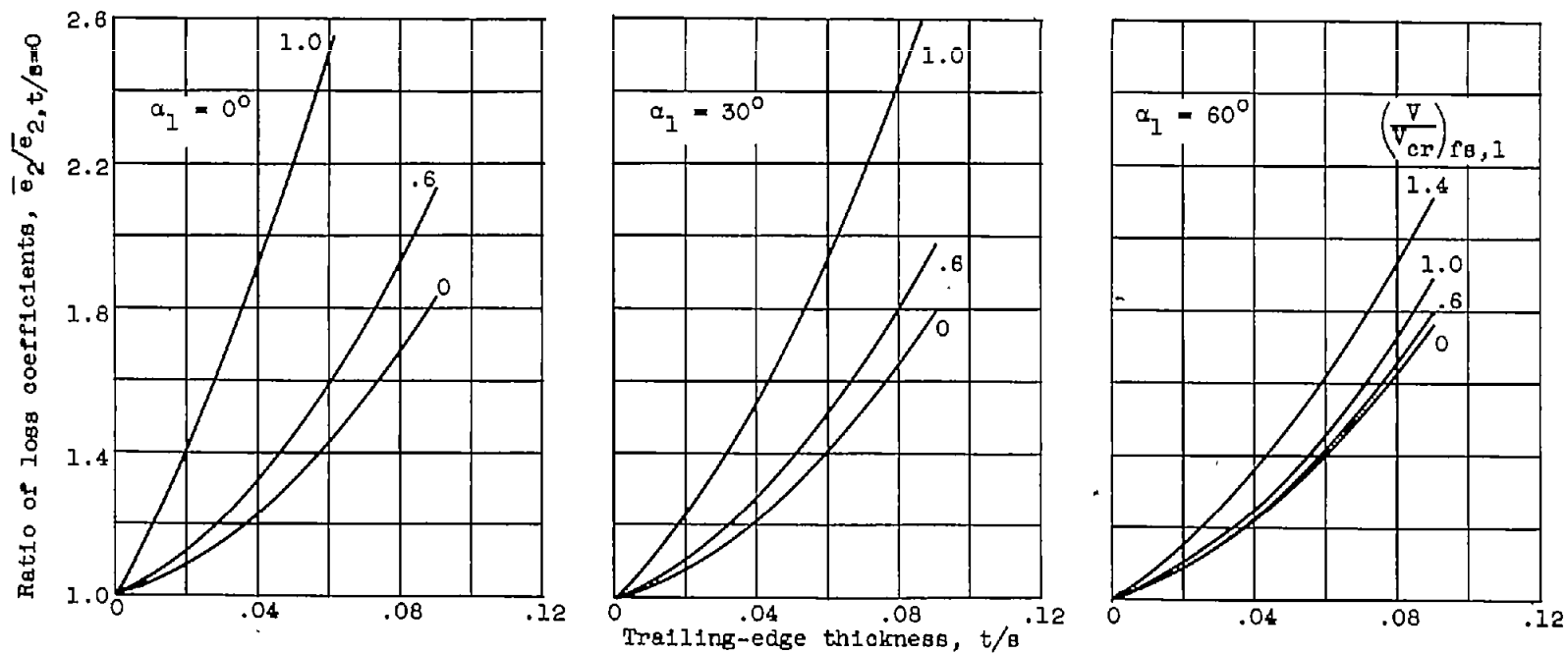


Figure 7. - Effect of trailing-edge thickness on over-all loss coefficients for compressible-flow conditions. $\theta^* = 0.01$; $n = 0.25$.